July 10, 2004

Radar Detection of Buried Landmines in Field Soils

T.W. Miller[1], J.M.H. Hendrickx[1*], and B. Borchers[2]

Resubmitted for publication in

Vadose Zone Journal

1. Hydrology Program, Dept. of Earth & Environmental Science, New Mexico Tech, Socorro, NM 87801
2. Dept. of Mathematics, New Mexico Tech, Socorro, NM 87801

- Corresponding Author: hendrick@nmt.edu

Radar Detection of Buried Landmines in Field Soils

ABSTRACT

The contrast in the dielectric constant between a landmine and the surrounding soil is one of the most important parameters to be considered when using ground penetrating radar (GPR) for landmine detection. For most geologic materials the dielectric constant lies within a range of 3-30, with dry sand at the lower end of this range at about 3-5. Nonmetallic antitank landmines have dielectric constants within a range of about 3-10 depending on their composition. A model was developed to predict whether or not field conditions are appropriate for use of GPR instruments. The predictions of this model were validated using GPR profiles in field soils with different soil textures at various soil water contents. Model predictions and field measurements provide convincing evidence that increasing the soil water content around a nonmetallic landmine can improve detection in sand and silt soils. However, data for the clay soils suggest that under elevated soil water conditions detection of nonmetallic landmines are not improved; instead radar images in these soils become worse with increasing soil water content. Data suggest that detection of metallic landmines also degrades with increasing soil water content in sandy soils. The field data are in agreement with the model predictions. Our experimental and model results demonstrate the great potential and the pitfalls of landmine sensors based on GPR. Knowledge of soil texture, dry bulk density, and water content are necessary to determine or predict whether soil conditions are suitable or not for GPR mine detection. The model presented here can be useful for making this determination.

INTRODUCTION

Sixty-five to 110 million landmines are scattered throughout 62 countries of the world, with Afghanistan, Angola, and Cambodia together totaling about 28 million mines (US Department of State, 1994). Detection and removal of these landmines is difficult because of the many variables involved, including soil type, climate, topography, and vegetation. Minefields are designed to be very complex since military engineers are taught to integrate minefields with natural obstacles such as steep slopes, watercourses, ditches, and dense vegetation (Ackenhusen et al., 2001). The expense of de-mining is also an important factor hindering landmine removal. With a cost estimated at $300 to $1000 per removal of each mine, the total cost for de-mining these countries is staggering (Ackenhusen et al., 2001).

No vadose zone contamination is worse than the landmine threat. The United Nations and the U.S. Department of State have declared that landmines are “one of the most widespread, lethal, and long lasting forms of pollution” (GICHD, 2003). Not only are thousands of persons killed, maimed, and injured each year but the social, economic, and environmental impacts of landmines are horrendous. In many developing countries the loss of fertile agricultural land and access to water points are among the most serious effects. Rural populations are driven onto increasingly fragile, marginal areas that leads to rapid land degradation (GICHD, 2003) and disturbance of the hydrological cycle.

In practice, current demining techniques involve the use of explosive sniffing dogs, metal detectors, and mechanical prods. Ground penetrating radar (GPR) is an alternative technology for landmine detection that has been extensively researched,

1 although it is not yet widely used in practice. GPR has the potential to be much more
2 effective than metal detectors in locating plastic cased landmines which have little or no
3 metal content.

4 Field experiments with ground penetrating radar have shown that soil conditions
5 can have a large effect on the performance of GPR systems for buried landmine
6 detection. Under some soil conditions the landmine signature is of high quality while
7 under others no signature can be detected at all. Fritzsche (1995) showed through
8 modeling that GPR signals at 900 MHz would be strongly attenuated in moist soils and
9 especially in clay soils. Trang (1996) found in both simulations and actual experiments
10 with a GPR operating in the 600-800 MHz frequency range that it was easier to detect
11 nonmetallic mines when the soil was moist. Johnson and Howard (1999) found that
12 elevated soil moisture actually improves detection by improving the contrast between
13 arid soils and plastic mines at the Energetic Materials Research and Testing Center (New
14 Mexico Tech, Socorro, New Mexico). Scheers et al. (2000) modeled the performance of
15 an ultra wide band GPR operating in the 1-5 GHz range for detection of metallic mines,
16 and found that the maximum depth at which the mine could be detected decreased as the
17 soil moisture increased. Yet, no studies have been conducted that in a systematic manner
18 evaluate the effects of soil texture and soil water content on radar signatures from land
19 mines. Therefore, the objectives of this paper are (1) to review a suite of models that can
20 be used for the prediction of soil electrical properties and radar responses under a wide
21 range of soil conditions; (2) to use these models to show the effects that soil texture and
22 water content can have on soil electrical properties; (3) to conduct field experiments for
23 validation of these models. This study includes plastic and metallic land mines with a

wide range of electrical properties. Hence, our results will be applicable not only to landmines but to other buried objects as well.

THEORY

The dielectric properties of a soil depend on a number of factors, including its dry bulk density, the texture of the soil particles (sand, silt, or clay), the density of the soil particles, typically about 2.66 g/cm^3 (Jury et al., 1991), the volumetric water content of the soil, the temperature, and the frequencies of interest (Hoekstra and Delaney, 1974; Topp et al., 1980; Ulaby et al., 1986). Research has also shown that the dielectric properties of soil depend on the amount of "bound water" which is in close contact with minerals in the soil (Wang and Schmugge, 1980; Dobson et al., 1985). Theoretical and empirical models of the dielectric properties of the different components of the soil have been combined into semi-empirical mixing models which can be used to predict the dielectric properties of field soils (Wang and Schmugge, 1980; Dobson et al., 1985; Wobschall, 1977; Peplinski et al., 1995).

For this study, we required a model that could predict both the real and imaginary parts of the relative electric permittivity for frequencies near the 900 MHz center frequency of the GPR system that we have used. The available data are the frequency, soil water content, and soil texture. Of the models mentioned above, only the model of Pelinksi et al. (1995) satisfies these requirements. This section summarizes the model of Peplinski et al. (1995), which covers the frequency range from 0.3 to 1.3 GHz. This model was based on an earlier model for dielectric constants in the 1.4 to 18 GHz range

by Dobson et al. (1985).

In this research we are interested in the attenuation of GPR signals in lossy soils. The static dielectric constant does not adequately represent the frequency dependent attenuation of GPR signals in these materials. Instead, we will use the complex relative electric permittivity. In the limiting case of a non-lossy soil with no frequency dependence the complex relative electrical permittivity is simply the dielectric constant.

The inputs to the model consist of the volumetric soil water content θ, the frequency *f*, the fraction of sand particles *S*, the fraction of clay particles *C*, the density of the soil particles ρ_S (a typical value is 2.66 g/cm^3), and the dry bulk density of the soil ρ_B. An empirically derived formula for effective ionic soil conductivity is the following

$$\sigma_{eff} = 0.0467 + 0.2204\rho_B - 0.4111S + 0.6614C . \quad [1]$$

The sand and clay fractions also enter the model through two empirically derived quantities β' and β", which depend on the soil type but are independent of the frequency and soil water content.

$$\beta' = 1.2748 - 0.519S - 0.152C \quad [2]$$

$$\beta'' = 1.33797 - 0.603S - 0.166C \quad [3]$$

Note that in these formulas, S and C are fractions, not percentages. E.g. If the clay content is 15%, then $C = 0.15$.

The real (ε'_{fw}) and imaginary (ε''_{fw}) parts of the complex relative electric permittivity (ε_{fw}) for the free water are given by a modified Debye model

$$\varepsilon_{fw} = \varepsilon'_{fw} - \varepsilon''_{fw} i \quad [4]$$

$$\varepsilon'_{fw} = \varepsilon_{w\infty} + \frac{\varepsilon_{w0} - \varepsilon_{w\infty}}{1 + (2\pi f \tau_w)^2} \quad [5]$$

and

$$\varepsilon''_{fw} = \frac{2\pi f \tau_w (\varepsilon_{w0} - \varepsilon_{w\infty})}{1 + (2\pi f \tau_w)^2} + \frac{\sigma_{eff}}{2\pi \varepsilon_0 f} \frac{(\rho_S - \rho_B)}{\rho_S \theta}. \quad [6]$$

In these formulas, ε_0 is the permittivity of free space, ε_{w0} is the static dielectric constant of water (80.1 at 20º C), $\varepsilon_{w\infty}$ is the high frequency limit of ε'_{fw} (4.9 at 20º C), and τ_w is the relaxation time of water (9.23×10^{-12} s at 20º C). The dielectric constant of the soil particles (ε_S) is given by the empirical model

$$\varepsilon_S = (1.01 + 0.44\rho_S)^2 - 0.062. \quad [7]$$

Finally, the real (ε') and imaginary (ε'') parts of the complex relative electrical permittivity for the bulk soil are estimated by

$$\varepsilon = \varepsilon' - \varepsilon'' i \quad [8]$$

where

$$\varepsilon' = 1.15\left[1 + \frac{\rho_B}{\rho_S}\left(\left(\varepsilon_S\right)^{0.65} - 1\right) + \theta^{\beta'}\left(\varepsilon'_{fw}\right)^{0.65} - \theta\right]^{\frac{1}{0.65}} - 0.68 \quad [9]$$

and

$$\varepsilon'' = \left[\theta^{\beta''}\left(\varepsilon''_{fw}\right)^{0.65}\right]^{\frac{1}{0.65}}. \quad [10]$$

The model was fitted to 399 measurements of the real and imaginary parts of the complex relative electrical permittivity of soil samples. The r-squared values were 0.985 for the real part (ε') and 0.940 for the imaginary part (ε'') (Peplinski et al., 1995).

As GPR signals travel through the soil, the attenuation is controlled by the complex relative electrical permittivity of the soil. The one-way attenuation loss in units of decibels (db) is given by

$$\text{Attenuation Loss} = 8.6855 d\alpha \qquad [11]$$

where d is the depth to the object from which the GPR signal is reflecting, and α is given by

$$\alpha = \frac{2\pi f}{c}\sqrt{\left(\frac{\varepsilon'}{2}\left(\sqrt{1+\left(\frac{\varepsilon''}{\varepsilon'}\right)^2}-1\right)\right)} \qquad [12]$$

where c is the speed of light in free space (2.997×10^8 m/s), and f is the frequency of the radar wave. Equation [12] assumes that conductive effects are negligible at the frequency of interest. If these effects are significant, then [12] may under predict the actual attenuation.

The models described in the theory section have been implemented in a MATLAB package. These MATLAB codes have been made available on the authors' web page at http://www.nmt.edu/~borchers/.

MATERIALS AND METHODS

To test the mathematical model described in the previous section, three field sites were chosen based on their soil texture. We required a variety of uniform soil water contents (10 to 40%); so to achieve these values, a sprinkler system was constructed. Simulant landmines were buried at each site, along with Time Domain Reflectometry probes for measuring soil water content. GPR measurements were then taken under a variety of soil water conditions at each of the three sites. The GPR data were analyzed and results compared with model predictions. Complete details of our experimental methods are presented in Miller (2002).

Sprinkler System

The sprinkler system was built out of ½ inch PVC tubing in the shape of a square measuring 3 by 3 meters and 1 meter tall. Seven Rain Bird XS-360TS-1032 spray nozzles were spaced 30 cm apart along the center of the sprinkler system. The system was designed to wet our experimental sites in a uniform manner. For details we refer to Miller (2002).

Antitank Landmines

The simulant landmines used at the Socorro site were completely inert and composed of Dow Corning 3110 RTV Silicon Rubber. They are designed to simulate the NR26, an antitank landmine, which is a nonmetallic landmine and has dimensions of

30.0 cm in diameter and 11.5 cm in height. TNO Physics and Electronics Laboratory in the Netherlands manufactured these landmine simulants.

Real antitank landmines were used at the Yuma Proving Ground site. These landmines have been defused for safety, but still contain their explosive charges.

GPR System

The measurements described in this study were performed with a Sensors & Software PulseEKKO 1000 ground penetrating radar system. The system was operated with 900 MHz antennas. This puts our measurements well within the 0.3 to 1.3 GHz band considered in the model of Peplinski et al. (1995). To ensure consistent antenna location, a wooden frame was used to position the antennas. This frame ensured that the horizontal positioning of the antennas was consistent between each experiment. The frame positioned the antennas approximately 4 cm above the ground.

In practice, a commercial GPR of this particular type would not be used for landmine detection. Most of the systems that have been field tested make use of radar in a "look ahead" configuration. However, we were limited in this research by the capabilities of the available GPR system.

Signal Processing Techniques

Seismic Unix was used for all the post data collection image processing. Seismic Unix is a signal processing software package developed by the Center for Wave Phenomena at the Colorado School of Mines (Stockwell and Cohen, 2001). A zero-phase, sine-squared tapered filter was applied to each image in the form of a highpass filter. Significant

ground bounce appeared in the upper part of each GPR profile. This was caused by the signal bouncing off the ground and ringing between the transmitting and receiving antennas. To delete this noise from the images the amplitude over this portion of the traces was set to zero.

Field Sites

Three field sites were chosen based on their soil texture: sand, silt, and clay. The sand and silt sites were located in the Sevilleta National Wildlife Refuge 20 km north of Socorro, NM, and the clay site was located in the Bosque Del Apache National Wildlife Refuge 40 km south of Socorro, NM. The sand soil had a composition of 95% sand, 2% silt, and 3% clay, and a dry bulk density of 1.60 g/cm^3. The silt soil had a composition of 2% sand, 66% silt, and 32% clay, and a dry bulk density of 1.30 g/cm^3. The clay site was located on the floodplain of the Rio Grande River in the Bosque Del Apache Refuge. This soil had a textural composition of 1% sand, 27% silt, and 72% clay and a dry bulk density of 1.54 g/cm^3. Using the U.S. Department of Agriculture classification scheme (Klute, 1986), the sand site soil was classified as a sand, the silt site soil was classified as a silty clay loam, and the clay site soil as a clay.

The U.S. Army's Yuma Proving Ground is located near the Arizona-California border, adjacent to the Colorado River, approximately 24 miles north of the city of Yuma, Arizona. The Countermine Testing and Training Range is located in the Kofa region of the area. In the Countermine Testing and Training Range there are two types of landmine lanes: the Handheld Detector Mine Lanes and the Vehicle-mounted Detector Mine Lanes. Both of these lanes have a mixture of nonmetallic and metallic, foreign and

domestic defused antitank landmines. The Yuma Handheld Detection Mine Lane has a soil composition of 80% sand, 14% silt, and 6% clay and is classified by the USDA classification scheme as loamy sand. The Vehicle-mounted Detector Mine Lane has a soil composition of 57% sand, 28% silt, and 15% clay and is classified as a sandy loam.

The following describes the general procedures used for burying the landmines at the sites in the Socorro, NM area. First, a 3 by 3 meter plot was cleared of any grass, shrubs, or other obstacles. Then the soil surface was leveled so that the surface was flat without any sloping edges. Inside this area an antitank landmine was buried 11 cm deep. Then a second antitank landmine was buried approximately 1.5 meters away from the first landmine also 11 cm deep. This second landmine had TDR probes buried above and below to measure the soil moisture around the landmine. The TDR probes were buried at 3 cm, 8 cm, 23 cm, and 28 cm below the ground surface. In this study we assume that the water content distribution measured around the mine instrumented with the TDR probes is equal to that around the mine without TDR probes. At the latter mine we measured radar responses without interference from the TDR probes.

RESULTS AND DISCUSSIONS

Model Predictions

In this section, the MATLAB program is used to predict the electric soil properties from the three field soils in Socorro, New Mexico. These predictions are used to demonstrate the effects of soil texture and water content on soil electrical properties.

Dielectric Constant versus Soil Water Content Predictions

Figure 1 shows how the complex relative electrical permittivity changes with soil water content for the three soils from the Socorro, New Mexico area. In this figure the predicted real part (solid lines) increases as the soil water content is raised, where the imaginary part (dotted lines) remains almost constant over the entire range of soil water contents. In this section, all model predictions are given for a frequency of 900 MHz, since that is the operating frequency of the GPR used in this study. The water contents used in the model are those measured in the field before and after water application with the sprinkler system (Miller, 2002).

Figure 1 predicts that the real part of the complex relative electrical permittivity will be 9.6 at 7% soil water content and 29.3 at 29% soil water content for the Sevilleta sand soil. It also predicts a value of 4.5 at 9% soil water content and 21.2 at 38% soil water content for the real part of the complex relative electrical permittivity of the Sevilleta silt soil. It further predicts a value of 4 at 5% soil water content and 26.9 at 38% soil water content for the real part of the complex relative electrical permittivity of the Bosque clay soil. The three lower and higher water contents represent the nominal water contents under, respectively, dry and wet soil conditions.

If a nonporous plastic landmine is buried in a sand, silt, or clay soil then as the soil water content increases, the bulk dielectric constant of the soil also increases, while the dielectric constant of the landmine remains the same (about 3). This elevation in the dielectric constant of the bulk soil will lead to a larger reflection coefficient (approaching unity), which in theory will lead to an improved image of the landmine. If the bulk dielectric constant and soil water content are the only factors examined, one may come to

the erroneous conclusion that for all soils landmine detection will improve with increasing soil water content because the dielectric constant contrast increases with elevated soil water contents. The next two sections explain the roles frequency and attenuation can have on the complex relative electrical permittivity.

Dielectric Constant versus Frequency Predictions

The complex relative dielectric permittivity of a soil also changes as a function of the frequency of the radar waves. Figure 2 shows how the complex relative electrical permittivity varies with frequency for the same Socorro soils at dry and wet soil water conditions.

In Figure 2, over the 0.3 to 1.3 GHz range, the imaginary part of the complex relative electrical permittivity for Sevilleta sand is almost invariant for both the dry and wet soil water conditions and does not appear to contribute a significant influence on the overall complex relative electrical permittivity. Similarly, the real part is also constant over this low frequency range and at the two soil water contents.

For the Sevilleta silt soil, the imaginary part of the complex relative electrical permittivity decreases significantly over the 0.3 to 1.3 GHz range for both the dry and wet soil water conditions.

For the Bosque clay soil over the low frequency range (0.3 to 1.3 GHz), the imaginary part or loss term is extremely significant when the soil is wet, changing by 7 over this range. When the soil is dry, the imaginary part of the dielectric constant decreases but is not as significant (changing by 1 over this range) as when the soil is wet.

High clay content in soils plays a significant role in elevating the imaginary part, as seen in the Bosque clay and Sevilleta silt soils.

Attenuation and Radar Response

From Equations [13] and [14] it is clear that radar wave attenuation should increase as the frequency of the radar increases and as the ratio of the imaginary part of the dielectric constant to real part increases. This ratio of imaginary to real part will generally increase as the soil water content is increased at a given frequency. Figure 3 shows the predictions for the attenuation over a range of soil water contents for the three Socorro soils at 900 MHz. From this figure, it is obvious that as the clay content of the soil increases, so does the amount of attenuation at a given soil water content. The Sevilleta sand soil (solid line), will attenuate about 20 db/m, where the Sevilleta silt soil (dashed line) will attenuate about 50 db/m, and the Bosque clay soil (dotted line) will attenuate about 65 db/m at 40% soil water content. Figure 4 shows how changes in frequency relate to radar wave attenuation. As frequency increases, the attenuation of the GPR signal in sand, silt, and clay soils increases rapidly.

Field Results

This section presents GPR wiggle trace plots of non-metallic simulant landmines as well as non-metallic and metallic landmines buried in the field soils described. However, before the field data is presented a brief introduction and explanation of how GPR detects buried objects is presented. Figure 5 (A) shows a radar system being moved along the surface of the earth with numbers 1 through 5 representing locations where traces are

collected. Figure 5 (B) shows the resulting wiggle trace plot representing the two dimensional cross-section of the buried landmine. In this figure, tracing out the first arrivals from the buried landmine at each trace forms a hyperbola, shown in Figure 5 (B). This hyperbola shape is formed because the first arrivals at points 1 and 5 take the longest time, the first arrivals at points 2 and 4 take an intermediate time, and the first arrival at point 3 takes the least amount of time to reflect off the mine. In the following images this hyperbola shape is seen in some of the images; however, a line has not been drawn to represent this feature.

In practice, the GPR signal is not radiated in all directions with equal power. As the real part of the relative dielectric permittivity increases, the beam is increasingly focused downward. As a result, the tails of the hyperbola are less prominent in situations where the dielectric constant is high.

In interpreting these graphs, it is also important to note that the vertical axis is travel time (in ns), not depth. Conversion to depth requires knowledge of the locations of the GPR antennas and the velocity of the GPR signal in the soil. This can be difficult because neither factor is known precisely. In practice, we were not able to precisely position the antennas, so travel times and depths are not strictly comparable between our experiments. For further discussion of these issues, see Miller (2002). We can generally expect that the velocity of the GPR signal in the soil will decrease as water content and the real part of the dielectric constant increase. Since the velocity of the GPR signal decreases under these circumstances, the travel time typically increases. This pattern is seen in most of the following results.

Socorro, NM Test Sites – Simulant Nonmetallic Landmines

Figure 6 shows a series of profiles of buried landmines in the three Socorro soils. The first image is a profile of the simulant landmine when the volumetric soil water content above the landmine is at 7%. The hyperbolic feature seen between the 20th and the 40th trace indicates the buried simulant landmine. The profile to the right of this is the same site after the volumetric soil water content above the landmine was raised to 29%. The landmine is again indicated by the hyperbolic feature and seen directly under the 20^{th} trace mark. These profiles clearly demonstrate that raising the volumetric soil water content of dry sandy soils can enhance the ability of the GPR to image landmines, which is in agreement with what our model predicts.

Figure 6 also shows two GPR wiggle trace plots of the Sevilleta silt loam site. The first profile was imaged at approximately 9% volumetric soil water content. The landmine in this profile is difficult to see, showing only a slight indication of a hyperbola between the 20^{th} and 40^{th} trace mark. This is because of the low contrast between the dielectric constant of the soil and the dielectric constant of the landmine. The second profile was imaged after raising the volumetric soil water content above the landmine to 38%. This image shows a very clear hyperbola directly under the 20^{th} trace mark. These figures demonstrate that for dry silt loam soils, the image of buried landmines can be improved by increasing the soil water content above the landmine.

Applying water to dry clay soils, however, does not enhance detection. The third row in Figure 6 shows two GPR wiggle trace plots from the Bosque Del Apache clay soil site. The first is an image taken during dry field conditions, with 5% volumetric soil water content above the landmine. The landmine is detectable under the dry clay soil

conditions shown in this figure. The hyperbolic feature directly below the 35th trace mark on the horizontal scale indicates the location of the landmine in this image. The second profile shows an image of the same Bosque clay soil after infiltrating a total of 2700 liters of water, raising the volumetric soil water content to 42% around the landmine. After application of large amounts of water, the landmine is clearly invisible to GPR. This is expected due to the extremely large attenuation in the wet clay, as our model suggests.

Yuma, AZ Test Sites – Nonmetallic Landmines

In this section the results from the Yuma Proving Ground landmine test lanes are presented. The four profiles seen in Figure 7 show GPR images of buried nonmetallic antitank landmines from the Handheld test range under both dry and wet soil conditions. The first profile in Figure 7 is a wiggle trace plot of a VS – 1.6 antitank landmine buried 7.62 cm deep in dry loamy sand soil. The VS – 1.6 is a low metal antitank landmine and contains a high explosive main charge with a surrogate RTV-3110 silicon rubber booster. The detonator shaft is the only metallic component of the landmine. In this profile a small reflection from the top of the landmine can be seen at the 34^{th} trace. The contrast in the dielectric constant between the landmine and the surrounding soil is not large enough to produce a significant reflection, so detection is difficult. The second profile is an image of the same landmine after the soil water content was raised to 26%. A stronger reflection is produced from the landmine and detection is enhanced through watering the soil.

The second row presents images of a VS – 2.2 nonmetallic antitank landmine buried 7.62 cm deep in dry loamy sand. The VS – 2.2 is very similar to the VS – 1.6 in dimensions and composition, and only differing in its thickness. The radar image of this landmine is similar, showing a small reflection under dry field conditions (See first image, second row in Figure 7). When the soil around the landmine is wet, a stronger reflection is produced from the surface of the landmine and the hyperbolic limbs can be seen extending outward (See second image, second row in Figure 7.)

Yuma, AZ Test Sites – Metallic Landmines

Figure 8 presents GPR images of two metallic antitank landmines. The first image in the upper row is of a TM62M metallic landmine buried in loamy sand soil. This figure shows a very strong reflection from the landmine when the soil is dry, since metallic landmines should produce perfect reflection because their reflection coefficients are equal to unity. The second profile is a radar image of the same landmine after the soil water content was raised to 26% above the landmine. The landmine in this figure would most likely not be detectable with GPR at greater soil water contents. . Metallic landmines have dielectric constants that are very large, approaching infinity, so the contrast between these types of landmines and the soil is also very large which should always produce significant reflections. However, as seen in this example applying water in certain situations will not enhance detection, rather it produces the opposite effect.

The bottom row in Figure 8 shows two images of a M15 metallic antitank landmine buried in a sandy loam soil. The metallic landmine in this figure produces a very clear reflection when the soil is dry. This is due to the large dielectric contrast

between the mine and the soil and the low attenuation in this dry soil. After the soil water content was increased to 23% above the mine, the image quality decreases. In particular, the reflection is less strong, and the hyperbola is narrower. This is the result of increased attenuation caused by the elevated soil water conditions. Although the velocity of the GPR signal is somewhat slower in the wetter soil on the right, the reflection of the mine appears earlier in time. We believe that this is simply due to differences in the antenna positioning between the two measurements.

SUMMARY

The goal of this study was to test the ability of ground penetrating radar to locate buried antitank landmines in field soils of different textures at varying levels of soil water content. To accomplish this, the expected response of the radar system was predicted using semi-empirical equations from the literature. Then a ground penetrating radar system was tested in various field soils and at various soil water conditions with a diversity of real and simulant antitank landmines. Our work has led to the following conclusions.

In sand and silt soils, the Peplinski model predicts that at 900 MHz the real part of the complex relative electrical permittivity will increase rapidly as the soil water content is increased. Since the dielectric constant of the mine remains constant, the contrast between the mine and the soil will also increase rapidly. This suggests that for these soils at elevated soil water conditions, there will be enough dielectric contrast to detect

landmines. In addition, the total attenuation for these types of soils is relatively low, so it will not hinder detection of landmines.

In clay soils at 900 MHz, the real part of the complex relative electrical permittivity increases rapidly as the soil water content is increased from dry soil to wet soil. However, the total attenuation in clay soils is very large, approaching 65 db/m at 40% soil water content. This suggests that landmine detection will not improve at elevated soil water conditions in this type of soil due to the strong attenuation.

GPR profiles of buried simulant nonmetallic antitank landmines in sand and silt soils at 900 MHz become clearer as the soil water content is increased from dry to wet. GPR profiles of buried simulant nonmetallic antitank landmines in clay soils at 900 MHz do not become clearer as the soil water content is increased from dry to wet. GPR profiles of buried metallic antitank landmines in sand and silt soils at 900 MHz do not become clearer as the soil water content is increased from dry to wet.

This study on the physics of landmine-radar-soil systems demonstrates both the great potential and the pitfalls of landmine sensors based on GPR. Radar works well with nonmetallic mines in wet sand and silt soils and in dry clay soils whereas metallic mines are best detected in dry soils. Unfortunately, soil texture (e.g. Hendrickx et al., 1986; Wierenga et al., 1987) and water content (e.g. Hendrickx et al., 1990, 1993; Jaramillo et al., 2000; Yao and Hendrickx, 2001) can change over relatively short distances. Soil water content distributions around landmines exhibit a large temporal variability (Das et al., 2001; Rhebergen et al., 2002). Hendrickx et al. (2001) and Lensen et al. (2001) demonstrate how the spatial variability of electrical soil properties is caused by changes

in soil texture and water content. These factors should be considered prior to and during deployment of a GPR system for landmine detection.

Hendrickx et al. (2003) discuss how worldwide soil data bases can be used to predict soil electrical properties. Yet, there is no simple prescription for when GPR will be effective. Rather, the model discussed in this paper should be used to determine the likely dielectric contrast between mine and soil and the likely attenuation of the GPR signal. In conditions where the dielectric contrast is strong and attenuation is mild, GPR is likely to work well. In other cases, it might be possible to alter the soil water content so as to improve the dielectric contrast while keeping the attenuation at an acceptable level.

ACKNOWLEDGMENTS

This work is funded by grants from the Army Research Office (Project 38830-EL-LMD) and the U.S. Army Yuma Proving Ground. The authors would like to thank Dr. Russell S. Harmon, Senior Program Manager at the Army Research Office, for his valuable advice and support. We appreciate the support and hospitality of Mr. Lance Vander Zyl, Director Tropic Test Center, and Mr. Stephen Patané, Test Director Munitions & Weapons Division, during our field work at the U.S. Army Yuma Proving Ground.

REFERENCES

Ackenhusen, J.G., Q. A. Holmes, K. Colin, and J. A. Wright. 2001. IRIA State of the Art Reports: Detection of Mines and Minefields. Infrared Information Analysis Center, Ann Arbor, MI.

Das, B. S., J. M. H. Hendrickx, and B. Borchers. 2001. Modeling transient water distributions around landmines in bare soils. Soil Science. 166:163-173.

Dobson, M.C., F.T. Ulaby, M.T. Hallikainen, and M.A. El-Rayes. 1985. Microwave Dielectric Behavior of Wet Soil-Part II: Dielectric Mixing Models. IEEE Trans. Geosci. Remote Sens., GE 23:35-46.

Fritzsche, M. 1995. Detection of buried landmines using ground penetrating radar. Proc. SPIE. 2496:100-109.

Geneva International Centre for Humanitarian Demining (GICHD). 2003. A guide to mine action. Geneva, Switzerland. Pp. 209.

Hendrickx, J.M.H., P.J. Wierenga, M.S. Nash, and D.R. Nielsen. 1986. Boundary location from texture, soil moisture, and infiltration data. Soil Sci. Soc. Am. J. 50:1515-1520.

Hendrickx, J.M.H., P.J. Wierenga, and M.S. Nash. 1990. Variability of soil water tension and soil water content. Agric. Water Managem. 18:135-148.

Hendrickx, J.M.H., L.W. Dekker, and O.H. Boersma. 1993. Unstable wetting fronts in water repellent field soils. J. of Environmental Quality 22:109-118.

Hendrickx, J.M.H., B. Borchers, J. Woolslayer, L.W. Dekker, C. Ritsema, and S. Paton. 2001. Spatial Variability of Dielectric Properties in Field Soils. *In* Detection and

Remediation Technologies for Mines and Minelike Targets VI, A.C. Dubey, J.F. Harvey, J.T. Broach, and V. George, editors, Proceedings of the SPIE 4394:398-408.

Hendrickx, J.M.H., R.L. van Dam, B. Borchers, J. Curtis, H.A. Lensen, and R.S. Harmon. 2003. Worldwide distribution of soil dielectric and thermal properties. *In* Detection and Remediation Technologies for Mines and Minelike Targets VIII, R.S. Harmon, J.H. Hollloway, Jr., and J.T. Broach, editors, Proceedings of the SPIE 5089:1158-1168.

Hoekstra, P., and A. Delaney. 1974. Dielectric Properties of Soils at UHF and Microwave Frequencies. J. of Geophys. Res. 79:1699-1708.

Jaramillo, D.F., L.W. Dekker, C.J. Ritsema, and J.M.H. Hendrickx. 2000. Occurrence of soil water repellency in arid and humid climates. J. of Hydrology 231/232:105-114.

Johnson, P.G., and P. Howard. 1999. Performance results of the EG&G vehicle mounted mine detector. Proc. SPIE. 3710:1149-1159.

Jury, W. A., W. R. Gardener, and W. H. Gardener. 1991. Soil Physics. Wiley, New York.

Klute, A. 1986. Methods of Soil Analysis - Part 1 Physical and Mineralogical Methods. 2nd ed., Agronomy Monograph No. 9, Soil Science Society of America, Madison, WI.

Lensen, H.A., P.B.W. Schwering, G. Rodríguez-Marín, and J.M.H. Hendrickx. 2001. Soil moisture distributions around land mines and the effect on relative permittivity. *In* Detection and Remediation Technologies for Mines and Minelike Targets VI,

A.C. Dubey, J.F. Harvey, J.T. Broach, and V. George, editors, Proceedings of the SPIE 4394:417-427.

Miller, T.W. 2002. Radar detection of buried landmines in field soils. M.S. Thesis, Dept. of Earth and Environmental Science, New Mexico Tech, Socorro, New Mexico. Pp. 124.

Peplinski, N.R., F.T. Ulaby, and M.C. Dobson. 1995. Dielectric Properties of Soils in the 0.3-1.3-GHz Range. IEEE Trans. Geosci. Remote Sens. 33:803-807.

Rhebergen, J.B., H.A. Lensen, H.A., P.B.W. Schwering, G. Rodríguez-Marín, J.M.H. Hendrickx. 2002. Measurements and modeling of soil water distribution around land mines in natural soil. *In* Detection and Remediation Technologies for Mines and Minelike Targets VII, J.T. Broach, R.S. Harmon, and G.J. Dobeck, editors, Proceedings of the SPIE 4742:269-280.

Scheers, B., M. Acheroy, and V.A. Vorst. 2000. Time domain modeling of UWB GPR and its application on landmine detection. Proc. SPIE. 4038:1452-1460.

Stockwell, J.W., and J.K. Cohen. 2001. Seismic Unix User's Manual-Version 3.0. Colorado School of Mines, Golden, CO.

Topp, G.C., J.L. Davis, and A.P. Annan. 1980. Electromagnetic Determination of Soil Water Content: Measurements in Coaxial Transmission Lines. Water Resour. Res. 16:574-582.

Trang, A.H. 1996. Simulation of mine detection over dry soil, snow, ice, and water. Proc. SPIE. 2765:430-440.

Ulaby, F.T., R.K. Moore, and A.K. Fung. 1986. Microwave remote sensing : active and passive. vol. 3, Artech House, Dedham, MA.

US Department of State. 1994. Hidden Killers: The Global Landmine Crisis. Dep. of State Publication *10225*, Washington, DC.

Wang, J.R., and T.J. Schmugge. 1980. An Empirical Model for the Complex Dielectric Permittivity of Soils as a Function of Water Content. IEEE Trans. Geosci. Remote Sens., GE 18:288-295.

Wierenga, P.J., J.M.H. Hendrickx, M.H. Nash, L. Daugherty, and J. Ludwing. 1987. Variation of soil and vegetation with distance along a transect in the Chihuahuan desert. J. of Arid Environm. 13:53-63.

Wobschall, D. 1977. A theory of the complex dielectric permittivity of soil containing water, the semidisperse model. IEEE Trans. Geosci. Electron. 15:49-58.

Yao, T. and J.M.H. Hendrickx. 2001. Stability analysis of the unsaturated water flow equation: 2. Experimental Verification. Water Resources Research, 37:1875-1881.

FIGURE CAPTIONS

Figure 1. Dielectric constant versus soil water content predictions for Sevilleta sand, silt, and Bosque clay soils at 900MHz.

Figure 2. Dielectric constant versus frequency predictions for Sevilleta sand, silt and Bosque clay soils. The vertical axes have different scales.

Figure 3. Attenuation versus soil water content predictions for Sevilleta sand, silt and Bosque clay soils at 900 MHz.

Figure 4. Attenuation versus frequency predictions for Sevilleta sand, silt and Bosque clay soils. The vertical axes have different scales.

Figure 5. Conceptual illustration of radar reflection from buried landmine (A) and resulting GPR wiggle trace plot (B).

Figure 6. Wiggle trace plots of the simulant NR26 antitank landmine buried 11 cm below the ground surface in the Sevilleta sand, silt and Bosque clay soils imaged using a 900 MHz GPR system.

Figure 7. Wiggle trace plots of defused antitank nonmetallic landmines buried in the Yuma, Arizona soils imaged using a 900 MHz GPR system.

Figure 8. Wiggle trace plots of defused antitank metallic landmines buried in the Yuma, Arizona soils imaged using a 900 MHz GPR system.

Figure 1. Dielectric constant versus soil water content predictions for Sevilleta sand, silt, and Bosque clay soils at 900MHz.

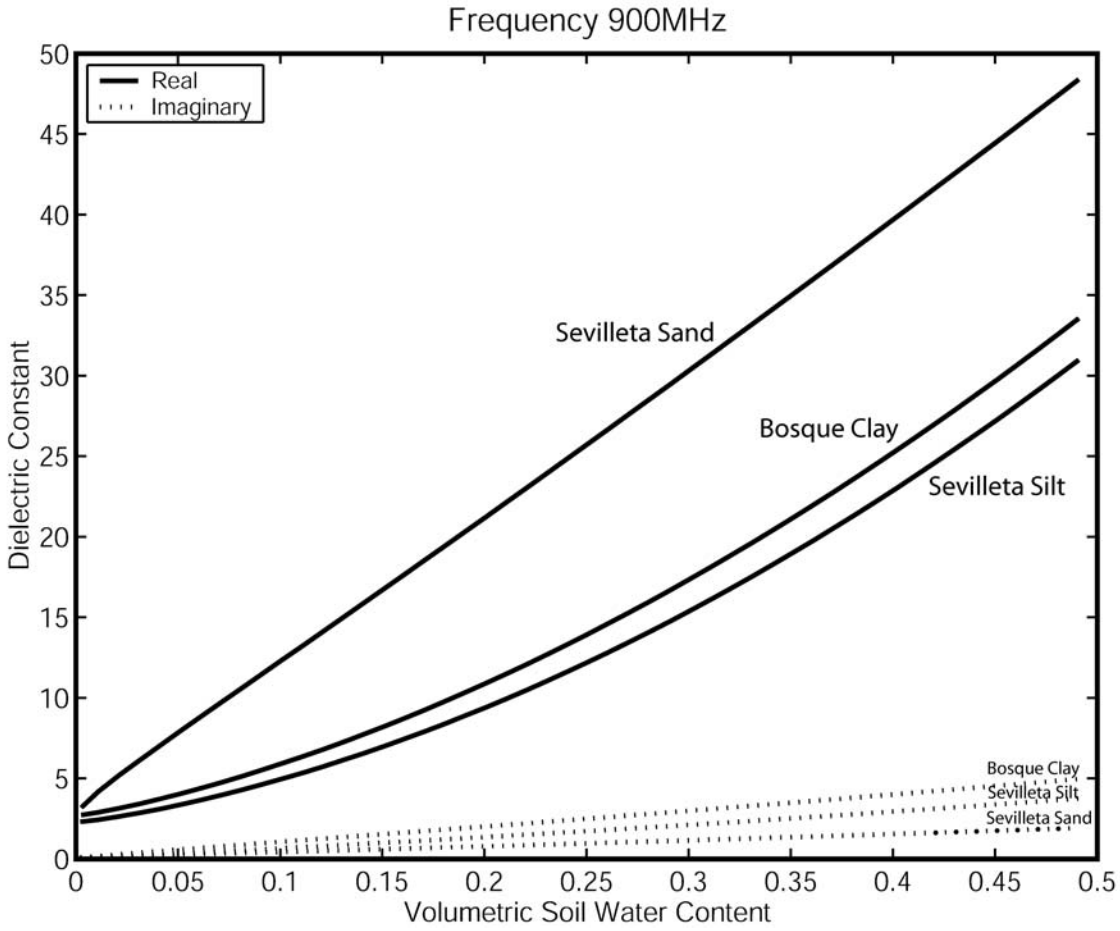

Figure 2. Dielectric constant versus frequency predictions for Sevilleta sand, silt and

ical axes h

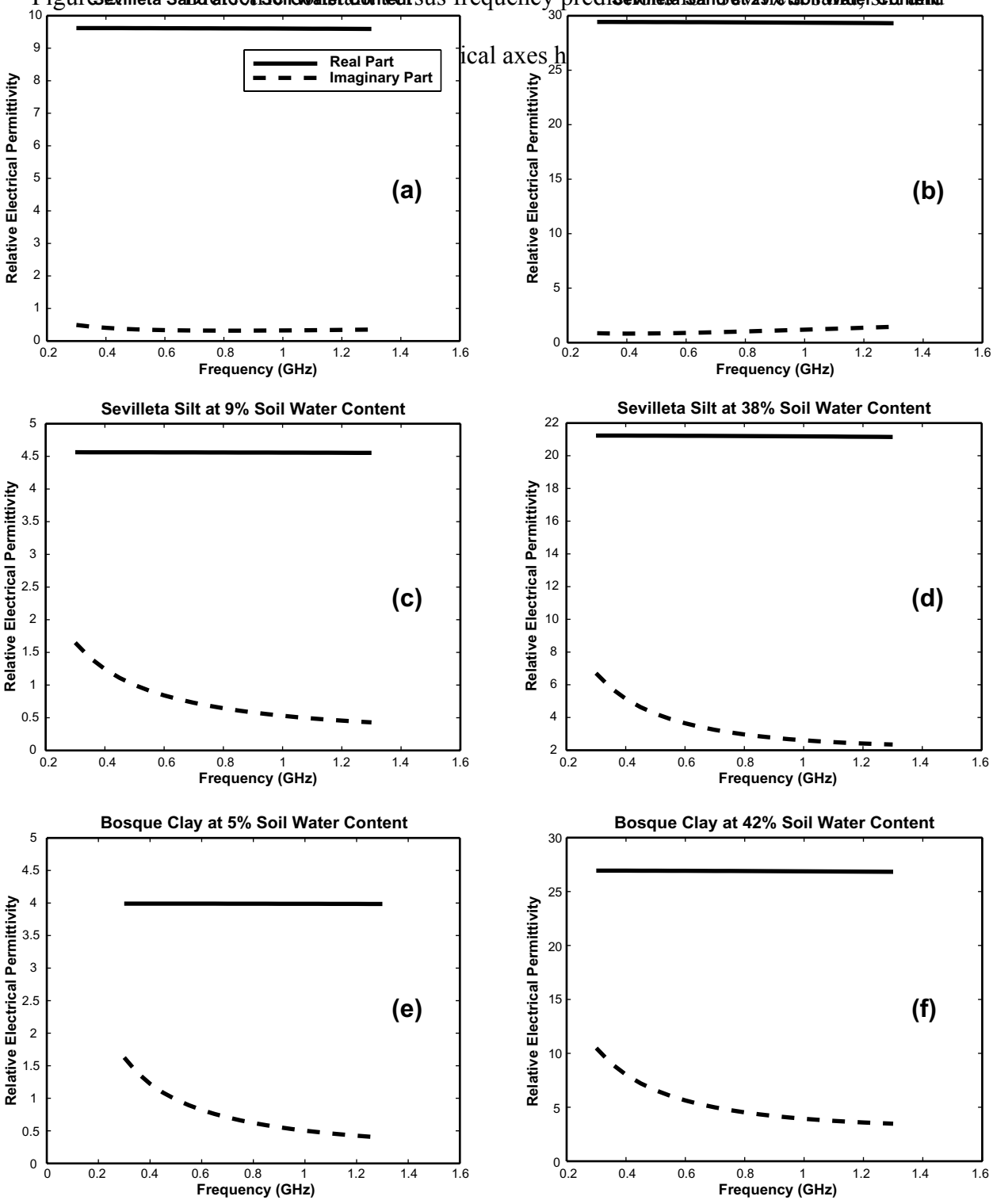

Figure 3. Attenuation versus soil water content predictions for Sevilleta sand, silt and Bosque clay soils at 900 MHz.

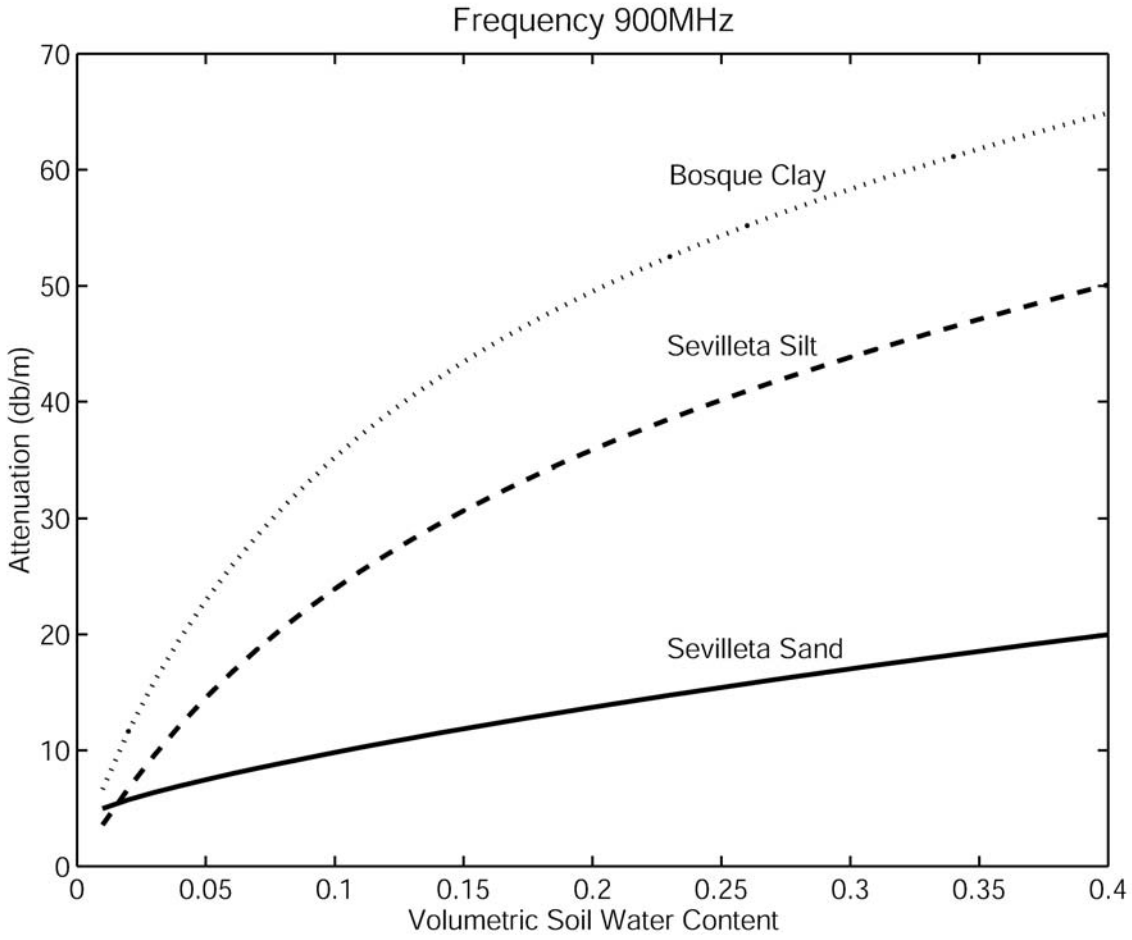

Figure 4. Attenuation versus frequency predictions for Sevilleta sand, silt, and Bosque clay soils. The vertical axes have different scales.

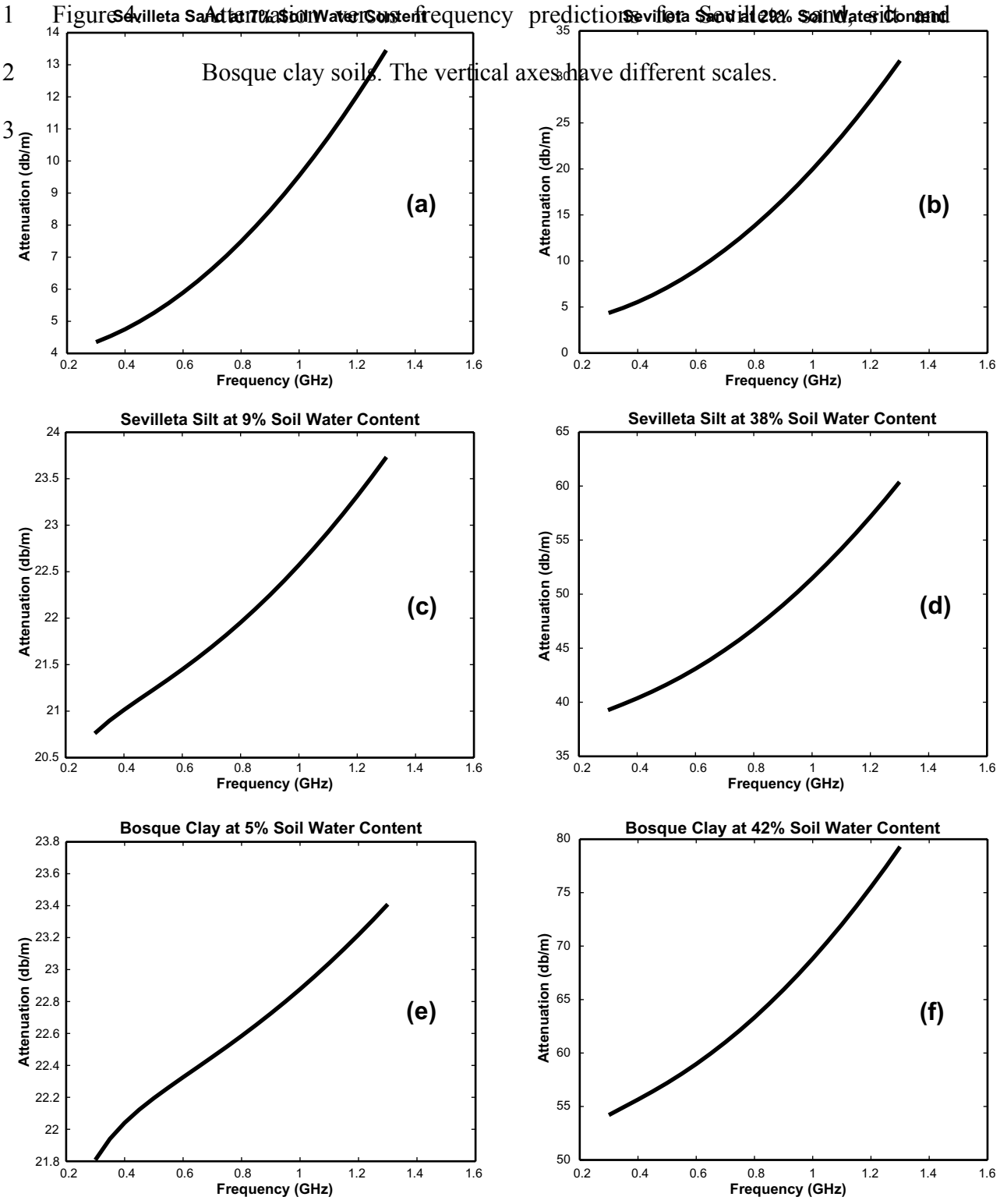

Figure 5. Conceptual illustration of radar reflection from buried landmine (A) and resulting GPR wiggle trace plot (B).

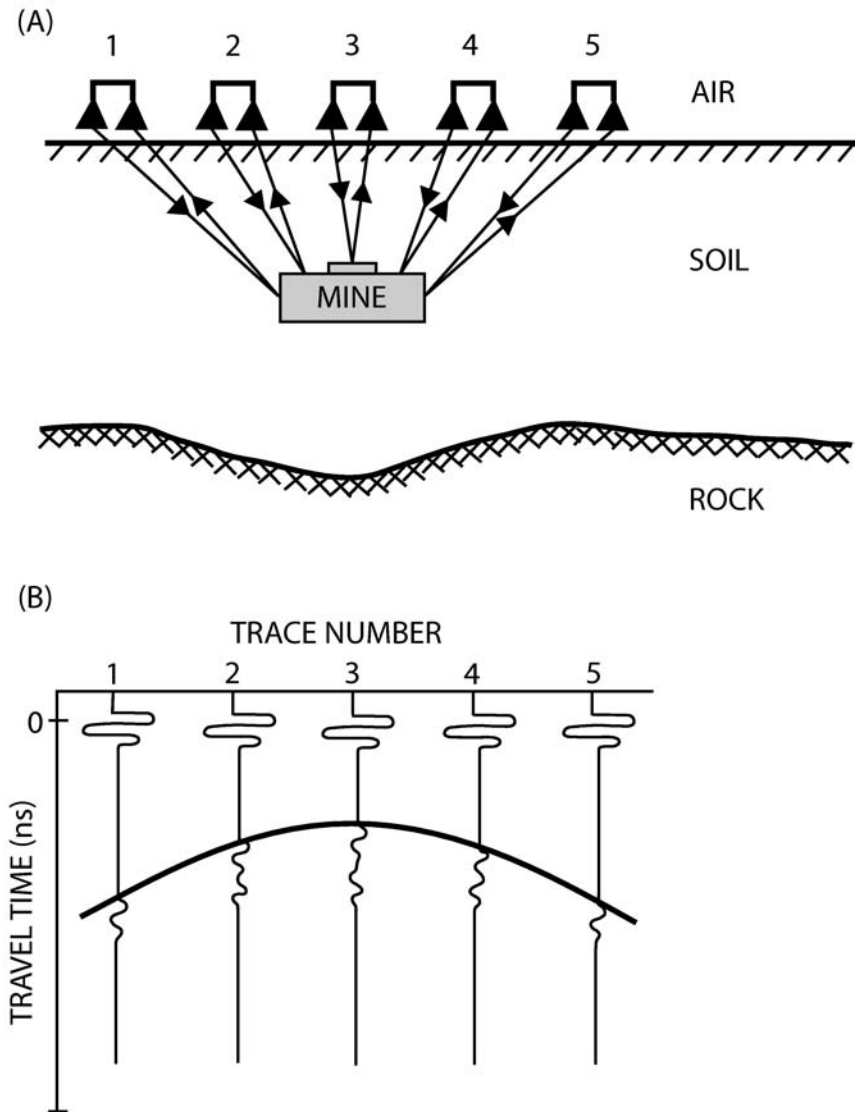

Figure 6. Wiggle trace plots of the simulant NR26 antitank landmine buried 11 cm below the ground surface in the Sevilleta sand, silt and Bosque clay soils imaged using a 900 MHz GPR system.

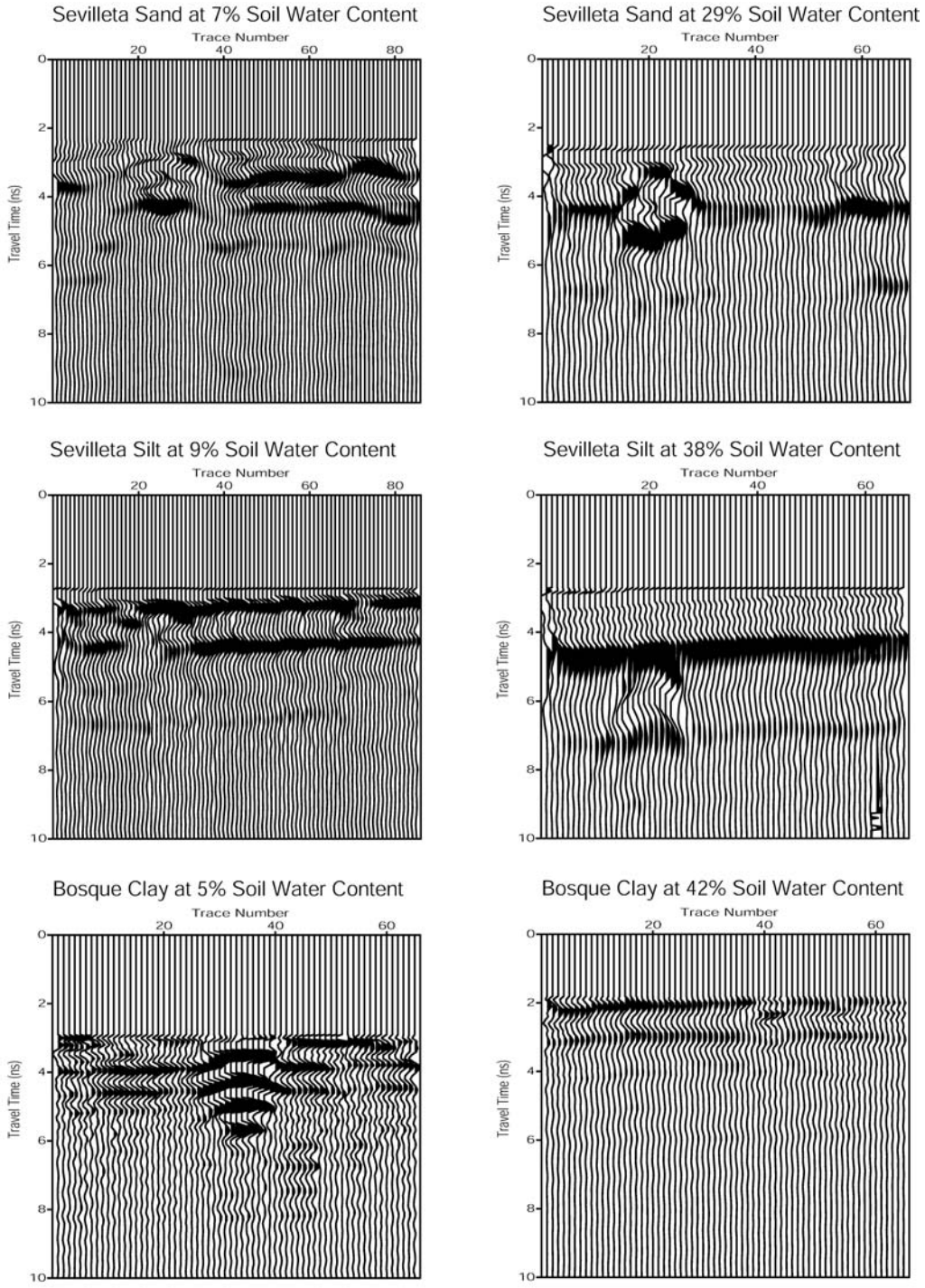

Figure 7. Wiggle trace plots of defused antitank nonmetallic landmines buried in the Yuma, Arizona soils imaged using a 900 MHz GPR system.

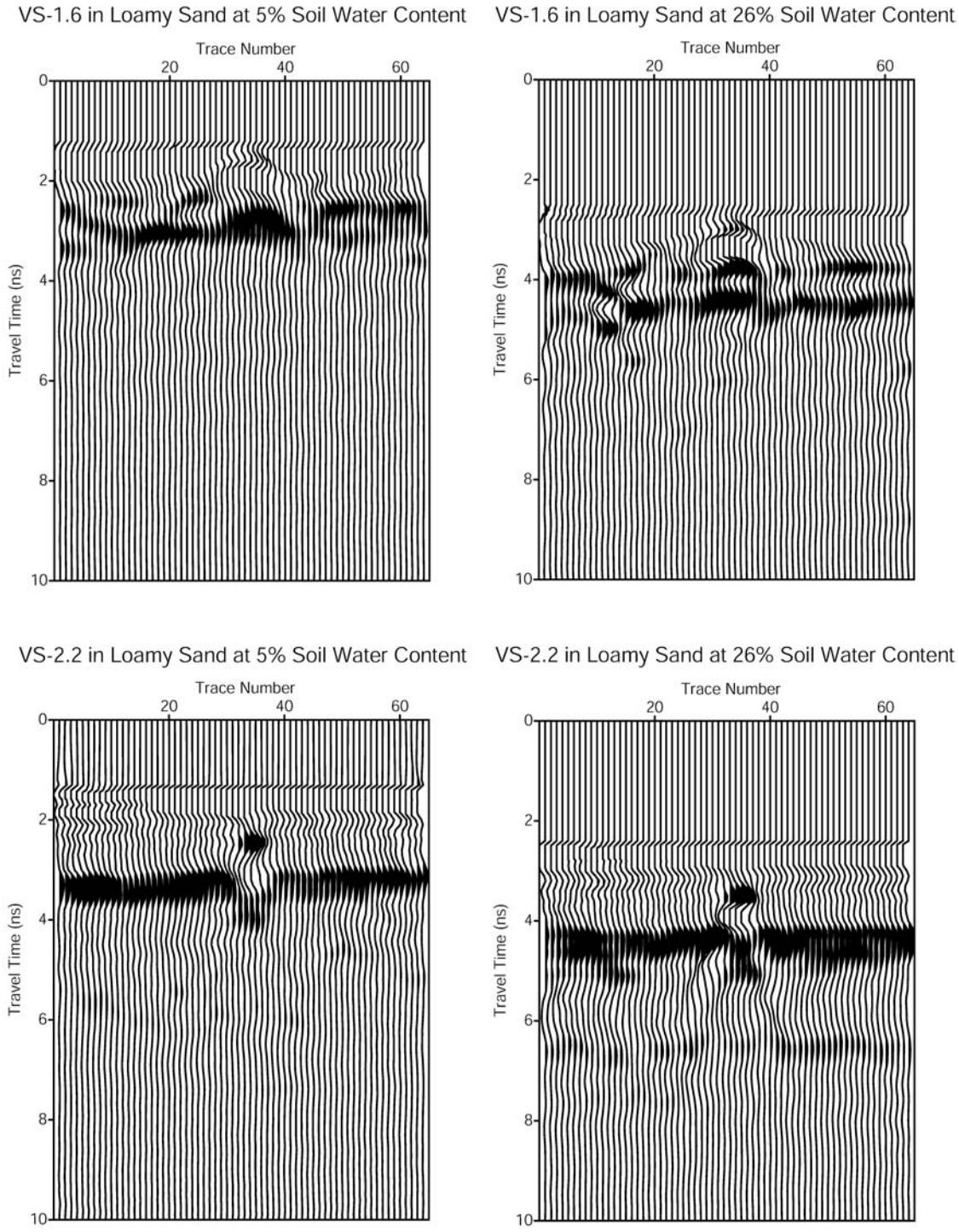

1 Figure 8. Wiggle trace plots of defused antitank metallic landmines buried in the

2 Yuma, Arizona soils imaged using a 900 MHz GPR system.

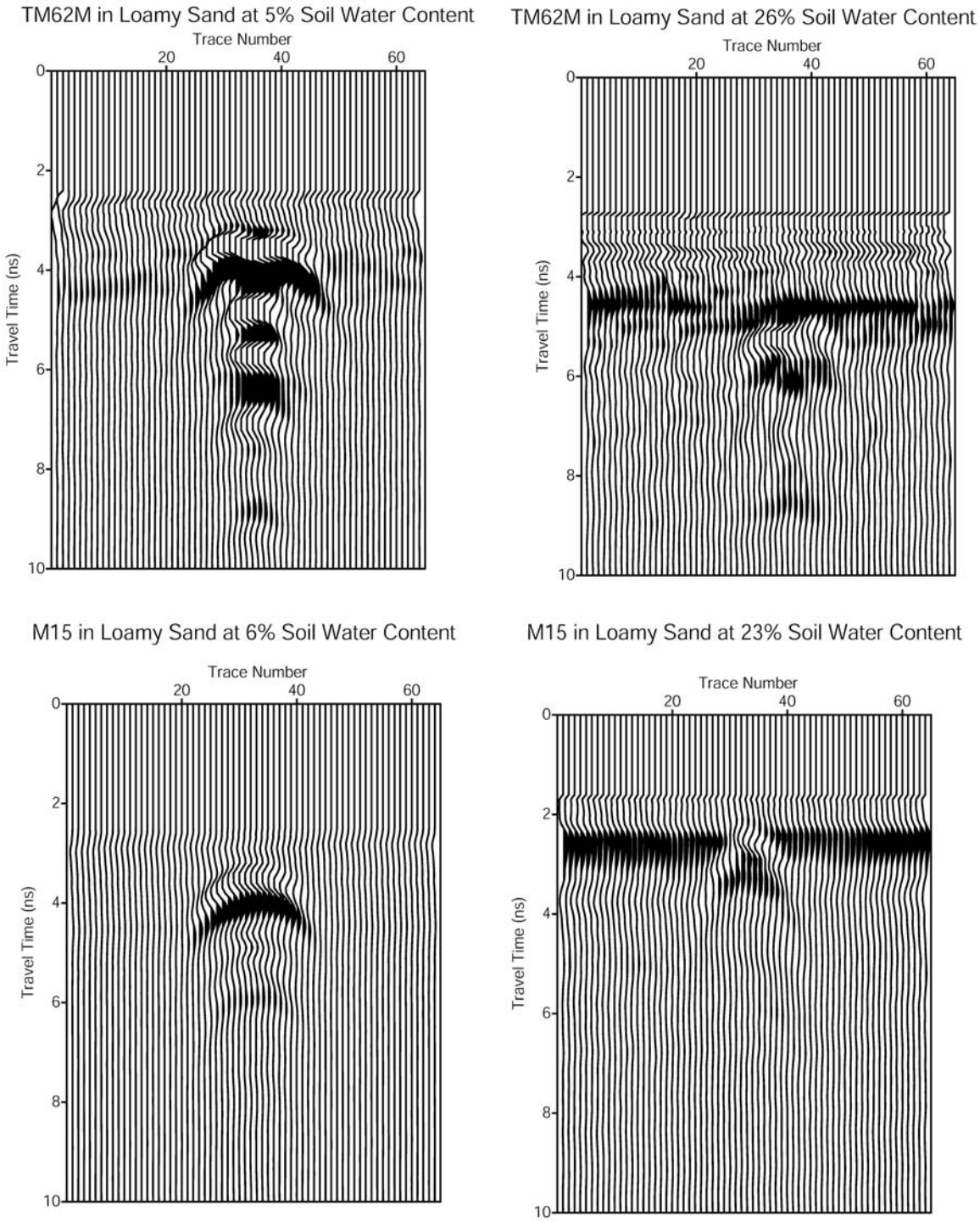

3